Role of Diblock Copolymers toward Controlling the Glass Transition of Thin Polymer Films

Hyunjoon Oh[†] **and Peter F. Green***[,†,‡]

Department of Materials Science and Engineering and Department of Chemical Engineering, University of Michigan, Ann Arbor, Michigan 48109

Received August 9, 2007; Revised Manuscript Received January 17, 2008

ABSTRACT: The physical properties of thin polymer films are often thickness, h, dependent, influenced by confinement and by interfacial interactions between the chains and the external interfaces. We show that the magnitude and film thickness dependence of the average glass transition temperature, T_g, of the polystyrene−silicon oxide (PS/SiO_x/Si) system are influenced appreciably with the addition of polystyrene-*b*-poly(methyl methacrylate) (PS-*b*-PMMA) diblock copolymers. The T_g can be "tailored" to increase, or decrease, with decreasing h or to remain independent of h. T_g shifts of as much of 35 °C are obtained for films of $h \approx 20$ nm. Additionally, we report that the critical micelle concentration, φ_{cmc}, of the copolymer in thin films is considerably larger than for the bulk; specifically, micelles form only beyond a critical film thickness, determined by the size of the chains and by the number of chains in the system. The h dependence of T_g is not influenced by the ϕ_{cmc} or by the number of micelles in this system.

Introduction

Thin polymer films are of considerable interest technologically in a diverse range of areas, from coatings and organic electronic devices to large-area screens, for reasons that include tunability of the chemical and physical properties, low production cost, ease of fabrication, and high flexibility. Organic light-emitting diodes (OLED),[1,2] organic photovoltaic cells (OPVC),[3–5] flexible displays,[6] and biosensors[7] represent specific examples of technologies in which thin polymer films are deployed. Use of thin polymer films in many applications necessarily involves the formation of interfaces with other materials. Consequently, a manifold of phenomena that influence processing and performance of these materials need to be understood: wetting,[8] instabilities,[9] viscoelasticity,[10,11] diffusion,[12–14] and glass transition temperatures (T_g).[15–38] The size-dependent properties, moreover, are often difficult to predict because they manifest the influence of confinement and of interfacial interactions between the material (chemical) constituents and the external interfaces. In this paper we are interested in the glass transition temperature, as it is of fundamental importance with regard to processing of polymers.

Considerable research, using a variety of experimental probes, dielectric spectroscopy,[15–18] X-ray and neutron reflectivities,[19–23] positron lifetime spectroscopy,[24] fluorescence spectroscopy,[25] shear-modulated scanning force microscopy,[26] Brillouin light scattering,[27–29] and spectroscopic ellipsometry,[30–37] reveals that the average T_g of films thinner than $h \approx 40$–60 nm may increase, or decrease, with decreasing h. For instance, the T_gs of polystyrene (PS) on silicon substrates, with native oxide layer, and poly(methyl methacrylate) (PMMA) on the gold-coated silicon substrate decrease with decreasing thickness,[28,30,31,33] while poly(2-vinylpyridine) (P2VP), tetramethyl bisphenol A polycarbonate (TMPC), and PMMA supported on silicon substrates, with native oxide layers, show an increase in T_gs with decreasing thickness.[21,25,30,32,34,35] A summary of the overall observations is that T_g decreases with decreasing film thickness, h ($\Delta T_g < 0$), if the film is freely standing or if the film resides on a substrate wherein the chain segments interact weakly (e.g., nonwetting) with the substrate; otherwise, if the interactions between the chain segments and the substrate are particularly strong, the glass transition increases with decreasing h ($\Delta T_g > 0$).

A number of theories have been proposed to explain the thickness-dependent behavior of T_g. One class of models can be classified as "interface-based" models; the phenomenological models of Keddie et al.,[30,31] DeMaggio et al.,[24] and Kim et al.[37] are such examples. In order to reconcile the decrease of T_g with decreasing h, Keddie et al. proposed the existence of a "liquidlike" layer, composed of comparatively high-mobility chain segments, possessing a high configurational entropy, at the free surface. DeMaggio et al. explained the T_g vs h behavior of the thin polymer film using the three-layer model: a "bulklike" interior layer, a liquidlike layer near the free surface, and "dead" layer near the substrate possessing lower mobility and higher T_g due to the interaction between chain segments and the substrate. Kim and co-workers also proposed a multilayer model. The work of Ellison and Torkelson[39] indicates that the T_g changes locally with distance from an interface, which lends some credence to the layered "interface-based" models. Theories based on the energy landscape (configurational entropy) models, and more restrictive models that compare local density profiles in thin films to the bulk to predict changes in T_g, yield results consistent with the experimentally determined thickness dependencies of T_g.

The foregoing models, however, are limited in that they do not provide a mechanism for the thickness dependence of T_g. The dynamic percolation model by Long and Lequeux[40] embodies a mechanism for the onset of T_g in thin films. In this model, thermal density fluctuations are responsible for the existence of spatially located domains characterized by "fast" and "slow" dynamics. Small differences in density are associated with significant differences in dynamics; this is due to the nonlinear dependence of dynamics on density in structurally disordered materials. Particles enter and leave the domains in order to preserve ergodicity; hence, the "fast" and "slow" domains are transient. The onset of percolation of the slow domains denotes the glass transition. The T_gs of thin films and bulk of the same material differ because the percolation thresholds in 2 and 3 dimensions are different. If the interactions between the chain segments and an interface are sufficiently

* To whom correspondence should be addressed.
[†] Department of Materials Science and Engineering.
[‡] Department of Chemical Engineering.

10.1021/ma071805v CCC: $40.75
Published on Web 02/29/2008

strong, hence reducing appreciably the configurational freedom of the chains, then the fraction of "slow" domains in the system increases, leading to an enhancement of the local T_g. The effect of interfaces on the T_g of the system is apparent: (1) the T_g decreases with film thickness for freely standing films because the fraction of "fast" domains increase due to the enhanced configurational freedom of the chains at the free surfaces; (2) the T_g generally increases with decreasing h, for films in contact with hard "walls" at both interfaces due to the increase in the number of "slow" domains. In systems where only one interface is supported, the thickness dependence of T_g would be dictated by the fraction of "slow domains", which is largely determined by the nature of the interactions between the chains and the substrate.

There have been a number of experiments devoted to understanding the influence of a second component on the T_g of a homopolymer system. These have included experiments on homopolymer/homopolymer blends;[34,35] here the effect of the second miscible component is to change the thickness dependence on T_g. In addition, the notion of a "self-concentration", responsible for local concentration fluctuations, is invoked to understand the behavior of this system.[41] The second class of systems is the nanoparticle/homopolymer blends,[36] where the nanoparticle has the effect of changing the thickness dependencies of T_g. The nanoparticles in principle increase the number of interfaces in the system and, due to the particle polymer interactions, increase the fraction of "slow" domains in the system and hence the T_g. It is evident from these systems that the second component has the effect of changing the thickness dependence of T_g, but for fundamentally different reasons.

In this paper we show that control of the interfacial interactions, through the use of block copolymers, provides a means by which the average T_g of the film can be "tailored". Because of their amphiphilic properties, diblock copolymers exhibit a natural tendency to segregate to the interfaces between melts and nonpolymeric interfaces[42–46] and to immiscible homopolymer interfaces,[47–50] leading to an increase of adhesion[51] and a decrease of interfacial tension.[52–55] We also show that the critical micelle concentration, φ_{cmc}, in thin films is significantly larger than in the bulk. In fact, there exists a critical film thickness beyond which micelles form; this critical film thickness is largely determined by the size of the diblocks, for systems in which one block strongly adsorbs to an interface, and the number of chains required to create a brush layer at the interfaces.

Experimental Section

Solutions of different weight fractions of PS-*b*-PMMA in PS were prepared by dissolving PS homopolymer, with nominal average molecular weight of 590 000 g/mol (Pressure Chemical Co., $M_w/M_n = 1.06$), and asymmetric PS-*b*-PMMA copolymer, with number-average molecular weight of 67 100 g/mol (Polymer Source Inc., $M_w/M_n = 1.09$), in toluene (Fisher Scientific Inc.). M_n of the PS component and M_n of the PMMA component of the copolymer are 46 100 and 21 000 g/mol, respectively. Before spin-coating onto silicon wafers, the solutions were mixed by an orbital shaker (MS 3 digital, IKA) for a day at 1000 rpm.

Films between ~16 and ~400 nm were spin-coated onto ⟨100⟩ oriented silicon substrates having a ~2 nm native oxide layer (Wafer World Inc.) by adjusting the concentration of the solutions and the spinning rate. The samples were then annealed under vacuum at 120 °C for 16 h to remove the solvent (this allowed sufficient time for the samples to reach an equilibrium state) and then quenched to room temperature. At this point the samples were uniform in thickness, with smooth surfaces (no dewetting). The T_gs were measured in a custom-made heating stage by using a variable angle spectroscopic ellipsometer (J.A. Woollam Co., Inc.). The ellipsometric parameters, Ψ and Δ, which are related to the change in the polarization, were measured at 10 °C intervals as the temperature

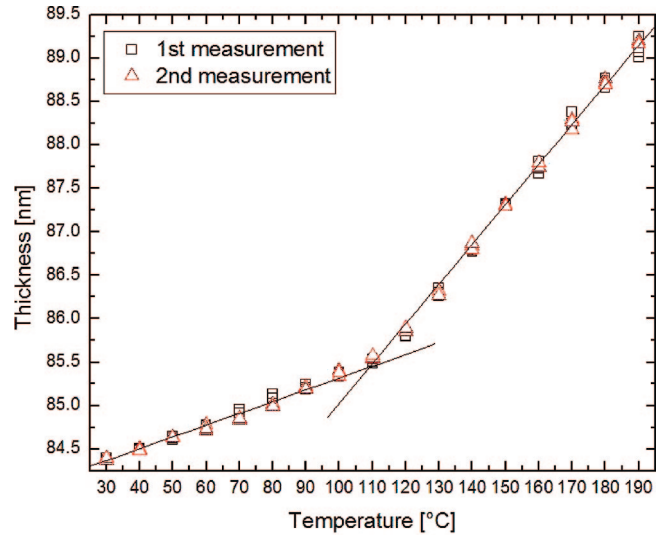

Figure 1. Typical dependence of thickness upon the surrounding temperature, shown via ellipsometry measurement. Data for pure PS with the thickness of 84.4 nm were plotted here. T_g was identified by the intersection of two extrapolated lines of first measurement (unfilled squares). A second measurement (unfilled triangles) was subsequently performed to examine the repeatability and the oxidative degradation effects.

was increased at a rate of 1 °C/min. In some experiments, the temperature was increased as much as 190 °C in order to get an accurate determination of T_g. Three different measurements were performed in the wavelength range of 400−750 nm at each temperature. For the analysis of the thickness, the data were fitted to the Cauchy/SiO_x/Si model over the entire measured spectral range using the WVASE32 ellipsometry analysis software (J.A. Woollam Co., Inc.). Experimental details are described elsewhere.[30–36] Typical data representing the temperature dependence of the thickness are shown in Figure 1. The plots show two distinctive regions: the glassy region at lower temperature and the rubbery region at higher temperature. T_g was determined by the break of the extrapolated tangent lines from these two regions of a first measurement. T_gs for all samples were collected in this way. We note that every sample including the pure PS-*b*-PMMA film exhibited a single break, i.e., one average T_g. A second measurement was carried out subsequently after cooling to room temperature and equilibrating for ~10 min. Since no reduction in thickness during each measurement, even after a second temperature cycle, was observed, it is safe to say that there were no effects of oxidative degradation during our experimental time scale.

The bulk T_gs of pure PS and pure PS-*b*-PMMA were determined using a Perkin-Elmer DSC7 differential scanning calorimetr (DSC). T_g was determined by the onset of a step transition at the second heating in a heating/cooling/heating (10 °C/−50 °C/10 °C per min) procedure. T_gs measured using DSC for PS homopolymer, PS blocks of PS-*b*-PMMA, and PMMA blocks of PS-*b*-PMMA are 101.8, 101.8, and 127.5 °C, respectively.

Scanning transmission electron microscopy (STEM) was used to examine the morphologies of the thin film samples. Films were spin-coated on glass slides and floated directly on the surface of deionized water. They were then placed on the silicon nitride membrane window grids (SPI supplies). After vacuum-annealing at 120 °C for 16 h, samples were exposed to vapor from aqueous RuO_4 solution for 5 min. This provides a contrast between the PS and PMMA because RuO_4 preferentially stains PS segments by attacking its aromatic ring. Z-contrast images of the samples were generated in the STEM mode under an accelerating voltage of 200 kV by the JEOL 2010F analytical electron microscope equipped with a high angle annular dark field (HAADF) detector. The contrast in HAADF imaging depends on the sample thickness and especially on the atomic number (Z). Therefore, PS domains having RuO_4

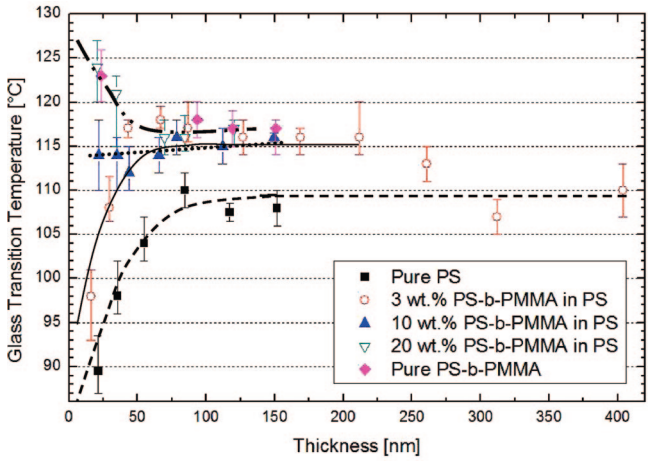

Figure 2. Film thickness dependence of the glass transition temperature for pure PS-*b*-PMMA (filled rhombi), pure PS (filled squares), and three different mixtures of PS-*b*-PMMA and PS. The lines are guides to the eye.

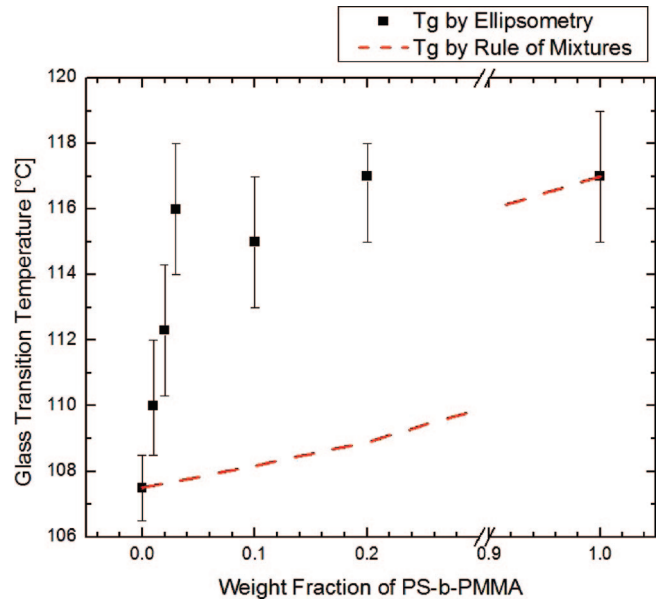

Figure 3. Glass transition temperature vs weight fraction of PS-*b*-PMMA diblock copolymer in the PS-*b*-PMMA/PS blend at constant thickness, ~120 nm. The broken line (- - -) represents the calculated T_gs by the rule of mixtures based on the volumetric ratio of PMMA blocks to the total mixtures.

elements were presented much brighter than PMMA domains in the STEM images.

Dynamic secondary ion mass spectroscopy (DSIMS) measurements were performed on a series of films. Films possessing thicknesses of ~250 nm were cast on the silicon and silicon nitride substrates. After annealing the samples under the same conditions to the previous experiments, ~30 nm blended films of 40:60 deuterated PS (Polymer Source Inc., M_w = 85 000 g/mol, M_w/M_n = 2.0) to PS (Pressure Chemical Co., M_w = 288 800 g/mol, M_w/M_n = 1.06) were added as a sacrificial layer on the top of the samples by a floating method. The DSIMS experiments were performed on a Physical Electronics 6650 quadrupole instrument at the University of California, Santa Barbara, by Dr. Tom Mates. A 6 keV, 100 nA Cs^+ primary ion beam was rastered over a 350 μm × 450 μm area, and negative secondary ions of hydrogen, deuterium, carbon, oxygen, and silicon were monitored from the center 20% of the crater area. The sputtering time was converted into the depth scale based on the thickness measured by the spectroscopic ellipsometer and the amount of time spent between interfaces.

Results and Discussion

The film thickness dependences of the glass transition temperatures for various mixtures of PS with PS-*b*-PMMA, by weight (0%, 3%, 10%, 20%, and 100%), are plotted in Figure 2. As shown in this figure, the T_gs of the pure PS samples thinner than ~50 nm decrease with decreasing thickness; otherwise, they remain independent of thickness for thicker films. These data are consistent with the published data on this system.[30,31] With the addition of only 3 wt % (ω = 0.03) of the PS-*b*-PMMA diblock to PS, the T_gs increase by ~10 °C ($T_g \approx$ 116 °C), throughout thicknesses of up to ~200 nm. For thicker films the T_g approaches that of bulk PS, as expected; 3 wt % PS-*b*-PMMA is insufficient to change the average T_g of a bulk film. The glass transition temperatures of films containing 10 wt % copolymer are independent of film thickness. When the samples contain 20 wt % copolymer, the opposite trend occurs; T_g increases with decreasing h, for h < 50 nm. Note that for thinnest samples, e.g., $h \approx$ 20 nm, the overall increase of T_g is ~35 °C; this is of significance as the PMMA component of the copolymer accounts for only ~6 wt % of the sample.

An assessment of the effectiveness of the copolymer toward changing the average glass transition temperatures of the films may be made by considering the T_g vs ω dependence of a film of thickness $h \approx$ 120 nm. The data in Figure 3 reveal that the T_g of the mixture increases by over 10 deg, to the value of the PS-*b*-PMMA copolymer, with only 3 wt % PS-*b*-PMMA. It is well-known that PS-*b*-PMMA diblock copolymers in PS hosts segregate to the silicon substrate.[42,46] The PMMA blocks possess a strong affinity for the native silicon oxide, through hydrogen bonding (O−H···O). The copolymers subsequently form a brush layer. Oslanec et al.[46] reported that the driving force for PS-*b*-PMMA adsorption is high enough to saturate the substrate with PS-*b*-PMMA chains if $P > 2N_{PS}$, where P and N_{PS} are the degrees of polymerization of the PS homopolymer and the PS block of the PS-*b*-PMMA, respectively. Since P (= 5673) ≫ $2N_{PS}$ (= 886), there exists a sufficiently strong driving force in our system. According to Green and Russell,[42] the number of copolymer chains per unit area at the interface increases rapidly with concentration of the copolymers up to certain critical concentration and becomes independent above that concentration. They concluded that this is due to the saturation at the substrate by the brush layer. Therefore, we can infer from the foregoing that the rapid increase of T_g with weight fraction of the diblock copolymer is associated with the interfacial segregation of the diblock copolymer.

The increase in T_g due to the interfacial segregation of the copolymers can be understood from the following. The mobility and configurational freedom of the copolymer chains near the substrate decrease due to this strong interaction, which, in the language of dynamic heterogeneity, leads to an increase in the fraction of "slow" domains in that region and hence the system. Once copolymers saturate the substrate or their substrate coverage reaches a certain threshold, the T_gs become independent of the concentration (Figure 3). This plateau in T_g occurs before the brush layer is completely formed; this becomes evident later when we discuss the morphology of the samples.

It is appropriate to consider the morphology of the samples in order to get a better appreciation of the structure–property behavior of this system. Because of the incompatibility between the PS and the PMMA components, the copolymers are anticipated to form micelles in the bulk at very low concentrations, far less than 1%, as the critical micelle concentration (cmc), $\varphi_{cmc} \sim \exp(\chi N)$. However, we see no evidence of micelle formation in samples thinner than 100 nm, even with copolymer concentrations of 20 wt %.

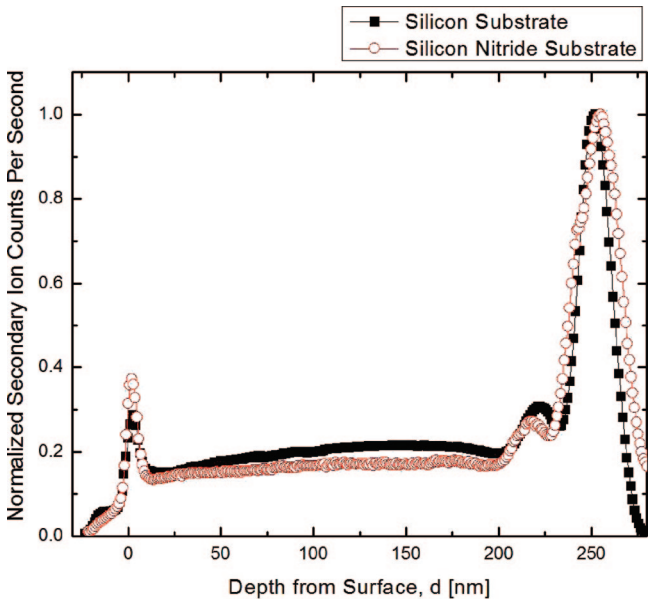

Figure 4. Normalized depth profiles of ^{16}O in 20 wt % PS-*b*-PMMA samples, supported by a silicon substrate (filled squares) and by a silicon nitride substrate (unfilled circles). ~30 nm sacrificial layers are placed on top of the samples which are ~250 nm in thickness. Here, $d \approx 0$ and 250 nm denote the interfaces of sacrificial layer/sample surface and sample/substrate, respectively.

Before we explain the basic reasons for the absence of micelles in these thin ($h < \sim 100$ nm) films, we begin by considering the morphology of thick samples ($h \approx 250$ nm) in which micelles are observed. Theoretical estimates of the micelle sizes are made and compared with the estimates. Silicon nitride (SiN) membranes (grown by low-pressure chemical vapor deposition (LPCVD)) were used for the substrates in the STEM studies to learn about micelle formation because the polymer film does not have to be removed from the SiN substrate for the STEM observations. This is not an issue as the degree of segregation of copolymers in the SiN and SiO_x/Si substrates is virtually identical, as shown in DSIMS profile in Figure 4. The narrow peak at the outer, free, surface is due to micelles, with the PMMA core and PS corona chains. In Figure 4, the oxygen peak of the brush layer is nearly hidden due to the strong signal from the native oxide of the substrate at $d \approx 250$ nm, though a kink is evident at $d \approx 240$ nm. The peak at $d \approx 220$ nm represents a layer of micelles; its full width at half-maximum exceeds the length of PMMA chains. Below, the micellar dimensions are estimated from a calculation of the micelle size, which would confirm that it does not represent the brush layer.

Figure 5a−c shows the STEM images of RuO_4-stained films of thickness $h \approx 250$ nm. In the images, the PMMA blocks of the copolymer appear darker than the PS because RuO_4 selectively oxidizes the PS component. The STEM image of the 20 wt % PS-*b*-PMMA thick film, before annealing, is shown in Figure 5a; the sample appears homogeneous. However, the images for the annealed samples (Figure 5b,c) possess dark spots, revealing the cores of micelles. This means that micelles in Figure 5b,c formed during annealing. The average radius of a micelle core (R_{core}) measured via STEM images is ~15 nm, yet the shortest distance between the centers of two adjacent, densely packed micelles is about 44 nm. Therefore, the radius of the micelle ($R_{micelle}$) may be about 22 nm, based on the supposition that these two neighboring micelles are in contact each other without deformation. We now briefly note that the bright spots in Figure 5b are overstained domains, which are sometimes observed in the STEM images of the PS homopolymer samples. The gray background includes both the PS homopolymer matrix and the PS-*b*-PMMA brush layer near the substrate.

The size of the micelles can be now estimated theoretically and compared with our observations. We begin by noting that the equilibrium structure of a micelle is determined by the minimization of the total free energy which can be approximated as a sum of three dominant contributions:[47,54,56,57]

$$F = F_{core} + F_{corona} + F_{interface} \quad (1)$$

where the first two terms represent the conformational free energies (or the stretching free energies) of the core and corona blocks and the last term is the free energy of the interface separating the core and the corona. Since the molecular weight of the PS block in PS-*b*-PMMA for our system, 46 100 g/mol, is much smaller than the molecular weight of the homopolymer PS, 590 000 g/mol, we can assume that the micelle possesses a dry corona layer; in other words, the corona layer, which consists of the PS blocks of PS-*b*-PMMA, has none or very little PS homopolymer. With the assumption that the interfacial region between the corona and the core is narrow compared to the corona and the core widths, and with the above assumption, Shull et al.[48] derived equations describing the radius of the spherical micelle. These equations may be rewritten as

$$R_{micelle}^{\ 3} = \frac{3}{4\pi} \frac{\sqrt{\chi} N_{cp} N_{core} a^3}{0.337 - 0.194 g^{1/3}} \quad (2)$$

$$R_{core}^{\ 3} = \frac{3}{4\pi} \frac{\sqrt{\chi} N_{core}^{\ 2} a^3}{0.337 - 0.194 g^{1/3}} \quad (3)$$

where $R_{micelle}$ and R_{core} are the radii of a micelle and a core, N_{cp} and N_{core} are the degrees of polymerization of the overall copolymer and its core segments, and g is the ratio of N_{core} to N_{cp}, i.e., N_{core}/N_{cp}. a and χ denote the statistical segment length and the Flory–Huggins interaction parameter between the core segments and the corona segments, respectively. Using eqs 2 and 3 and the set of parameters $N_{cp} = 651$, $N_{core} = 208$, $g = 0.3195$, $\chi = 0.0379$,[58] and $a = 6.9$ Å[59] (here, χ and a were calculated by assuming that they are independent of the symmetry of the diblock copolymer), $R_{micelle} \approx 21.6$ nm and $R_{core} \approx 14.8$ nm are obtained for the radii of the micelle and its core, respectively. These values are comparable to the values estimated by the STEM measurements.

We now discuss the reason the cmc in thin films is considerably higher than the bulk. No micelles were observed in 3 and 20 wt % PS-*b*-PMMA thin film ($h \approx 20$ nm) samples (see Figure 5d,e). In fact, no micelles are formed in films with thicknesses $h < 100$ nm. This can be rationalized by the fact that PS-*b*-PMMA chains in the thin films are initially forced to form the brush layer at the substrate before forming micelles due to the stronger driving force for interfacial segregation; the PMMA component of the copolymer resides at the oxide layer. The "brush" layer would be ~22 nm, based on the average diameter of the micelle. Therefore, a sample of $h \approx 100$ nm thick containing a 22 nm brush layer would need to contain roughly 22% (22 nm/100 nm) of copolymer chains to create a saturated brush layer. Since the thinner samples we examined had 20% or smaller weight fractions of chains, the brush layer remained unsaturated; hence no micelle formation. These observations can be confirmed by considering Figure 5f, which shows the image of the 20 wt % PS-*b*-PMMA sample with thickness gradient. The dark gray area in the upper left corner of the image where the film thickness is ~19 nm contains no micelles, as expected. However, in the lower right of the image, where the thickness of the film increases ($h > 100$ nm), micelles exist. Before ending this section, it must be emphasized that

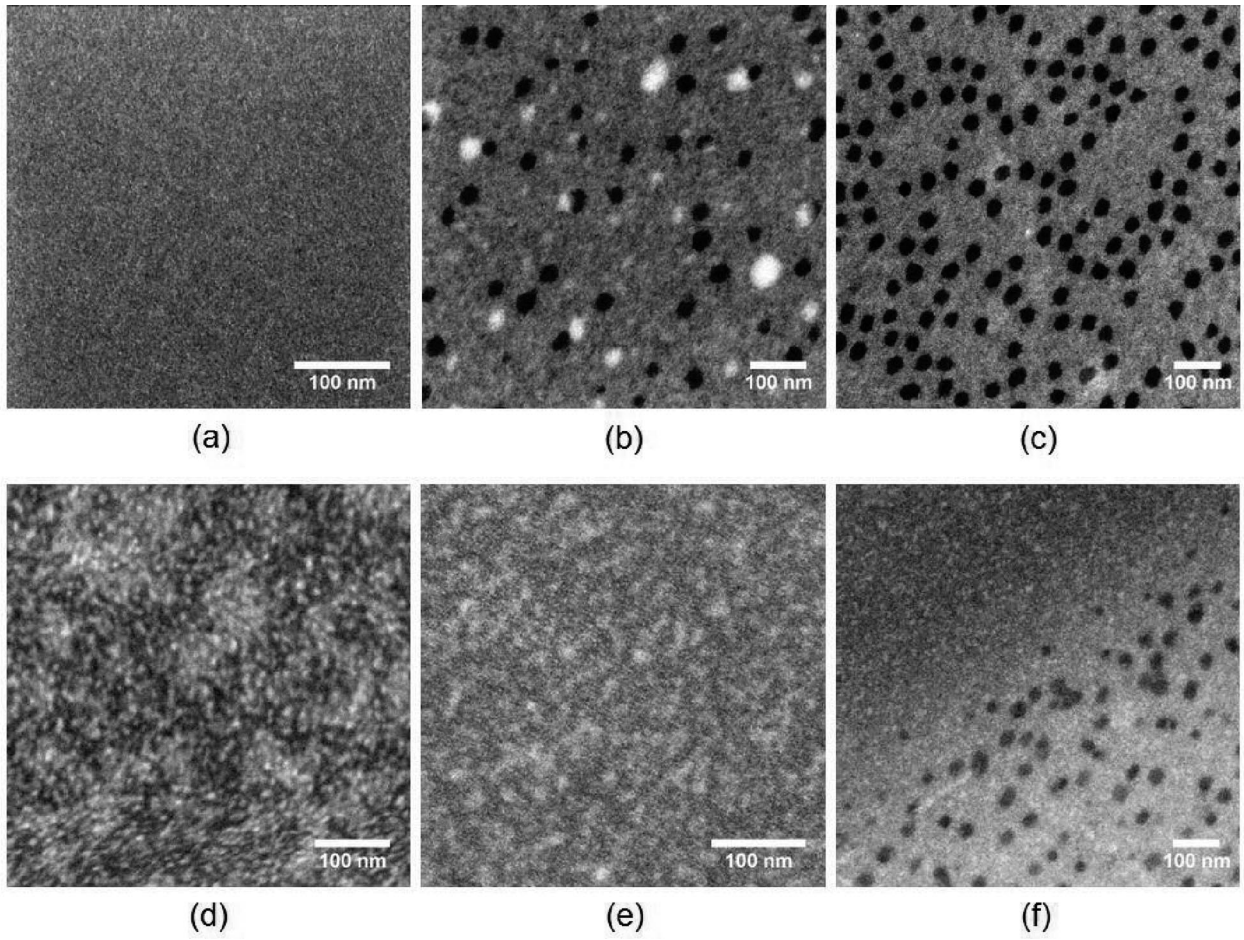

Figure 5. STEM images of RuO_4-stained samples on the silicon nitride window grids: (a) h (thickness) $\approx$ 250 nm, 20 wt % PS-*b*-PMMA as-cast sample; (b) $h \approx 250$ nm, 3 wt % PS-*b*-PMMA sample; (c) $h \approx 250$ nm, 20 wt % PS-*b*-PMMA sample; (d) $h \approx 19$ nm, 3 wt % PS-*b*-PMMA sample; (e) $h \approx 19$ nm, 20 wt % PS-*b*-PMMA sample; (f) $h \approx 19$ nm, 20 wt % PS-*b*-PMMA sample with thickness gradient.

when the films are sufficiently thick, the influence of the interface should diminish considerably and the behavior should approach that of the bulk, wherein φ_{cmc} should decrease considerably, as would the T_g. In the case of the 3 wt % PS-*b*-PMMA, the T_g approaches the bulk T_g for $h > \sim 250$ nm (cf. Figure 2). With regard to the effect on micelle formation, we see evidence of micelles in the 250 nm samples containing 3 wt % PS-*b*-PMMA, where 3 wt % PS-*b*-PMMA is not sufficient to form a complete, saturated, brush layer. The behavior of films of this thickness, and beyond, is clearly bulklike behavior. We further anticipate that as the interaction parameter, χ, increases in magnitude, this will enhance micelle formation in the interior of the system and will compete with the interfacial segregation. It should be clear that in sufficiently thin films φ_{cmc} is orders of magnitude larger than the bulk.

A mechanism for understanding the T_g dependence on h, based on the dynamic heterogeneity model, might be as follows. Recall that for freely standing films the chains in the vicinity of the free surfaces possess a higher degree of configurational freedom, and this has the effect of increasing the fraction of "fast" domains in the sample. This effect largely accounts for the fact that T_g always decreases with decreasing h in freely standing films, the difference in the percolation threshold in 3D and quasi-2D not withstanding. When one interface is constrained, the fraction of "slow" domains increases. Under these conditions it is the relative competition between the "fast" domains, associated with the free surface, and the "slow" domains, associated with the substrate interactions, that determine whether T_g increases or decreases with decreasing h. If the interactions between the chains and the substrate are weak, i.e., nonwetting, as is the case for PS and SiO_x/Si, then the dynamics associated with the "fast" domains dominate and T_g decreases with decreasing h. However, in cases such as PMMA or TMPC on SiO_x/Si, where the chain/substrates are strong, the effective number of "slow" domain induced in the system is sufficiently large, and T_g increases with decreasing h. In our system, the copolymers segregate to the interface due to the PMMA/SiO_x/Si interactions; the end result is an enhancement of the average T_g of the sample.

Conclusion

Film thickness dependencies of the average glass transition temperatures of thin polymer films are well documented. Typically, below a threshold film thickness, T_g may increase or decrease with decreasing h, depending on the polymer−substrate system (T_g decreases with decreasing h for freely standing systems). In the PS/SiO_x/Si system, T_g decreases with decreasing h, for $h < 50$ nm. We showed that with the addition of small quantities of an A-*b*-B diblock copolymer the thickness dependence of T_g could be "tailored". Changes in T_g of as much as 35 deg could be accomplished with the addition of the copolymer. The increase is associated with the increasing segregation of the diblock copolymers to the substrate to lower the free energy. The strong attraction of the PMMA for the oxide layer limits the configurational freedom and the mobility of the chains in the vicinity of the interface. On the basis of the dynamic heterogeneity model, this has the effect of increasing the fraction of "slow" domains in the system and hence the increase of T_g. There is a length scale over which the influence

of the interfaces on T_g becomes unimportant, and this becomes clear from the following. The influence of the interfacial activity of the copolymers on the average T_g of the 3 wt % PS-*b*-PMMA samples extends to samples with thickness on the order of 200 nm. Beyond this thickness, the T_g of the system becomes equivalent to the T_g of a bulk system, where the small concentration of copolymers (3 wt %) is not sufficient to change the T_g of the system.

We also showed that the critical micelle concentration in thin films ($h < 100$ nm) is orders of magnitude larger than the bulk. At equilibrium, diblock copolymers segregate to the substrate due to the preferential attraction of the PMMA component. The formation of the brush layer ensures the chemical potential of copolymer chains is the same throughout the system at equilibrium. The time scale for reaching equilibrium will depend on the film thickness and on χN. Further, there is the aforementioned length scale (film thickness effect) beyond which the system becomes bulklike, and so micelles are formed even at lower concentration sufficiently far from the substrate. In our system, the influence of the interface on the cmc of the system diminishes for films much thicker than 100 nm. In general, the critical micelle concentration of thin film homopolymer/copolymer systems is larger than the bulk due to the segregation of copolymers to an interface. A further study involving other systems is underway to develop some scaling rules.

Acknowledgment. Support for this research from the National Science Foundation #DMR 0601890 and from the US Department of Energy DOE#DE-FG02-07ER46412 is gratefully acknowledged. We thank Dr. Luciana Meli for STEM images and Dr. Tom Mates for DSIMS data. The JEOL 2010F Analytical Electron Microscope used in this study were funded by the National Science Foundation Grant #DMR 9871177.

References and Notes

(1) Tang, C. W.; VanSlyke, S. A. *Appl. Phys. Lett.* **1987**, *51* (12), 913–15.
(2) Baldo, M. A.; Thompson, M. E.; Forrest, S. R. *Nature (London)* **2000**, *403* (6771), 750–753.
(3) Tang, C. W. *Appl. Phys. Lett.* **1986**, *48* (2), 183–5.
(4) Yu, G.; Gao, J.; Hummelen, J. C.; Wudl, F.; Heeger, A. J. *Science* **1995**, *270* (5243), 1789–91.
(5) Peumans, P.; Uchida, S.; Forrest, S. R. *Nature (London)* **2003**, *425* (6954), 158–162.
(6) Sheraw, C. D.; Zhou, L.; Huang, J. R.; Gundlach, D. J.; Jackson, T. N.; Kane, M. G.; Hill, I. G.; Hammond, M. S.; Campi, J.; Greening, B. K.; Francl, J.; West, J. *Appl. Phys. Lett.* **2002**, *80* (6), 1088–1090.
(7) Heeger, P. S.; Heeger, A. J. *Proc. Natl. Acad. Sci. U.S.A.* **1999**, *96* (22), 12219–12221.
(8) de Gennes, P. G. *Rev. Mod. Phys.* **1985**, *57* (3), 827.
(9) Besancon, B. M.; Green, P. F. *Phys. Rev. E* **2004**, *70* (5), 051808–8.
(10) Alsten, J. V.; Granick, S. *Macromolecules* **1990**, *23* (22), 4856–62.
(11) Hu, H. W.; Granick, S. *Science* **1992**, *258* (5086), 1339–42.
(12) Frank, B.; Gast, A. P.; Russell, T. P.; Brown, H. R.; Hawker, C. *Macromolecules* **1996**, *29* (20), 6531–6534.
(13) Zheng, X.; Sauer, B. B.; Van Alsten, J. G.; Schwarz, S. A.; Rafailovich, M. H.; Sokolov, J.; Rubinstein, M. *Phys. Rev. Lett.* **1995**, *74* (3), 407–10.
(14) Zheng, X.; Rafailovich, M. H.; Sokolov, J.; Strzhemechny, Y.; Schwarz, S. A.; Sauer, B. B.; Rubinstein, M. *Phys. Rev. Lett.* **1997**, *79* (2), 241–244.
(15) Fukao, K.; Miyamoto, Y. *Europhys. Lett.* **1999**, *46* (5), 649–654.
(16) Fukao, K.; Miyamoto, Y. *Phys. Rev. E* **2000**, *61* (2), 1743–1754.
(17) Serghei, A.; Mikhailova, Y.; Huth, H.; Schick, C.; Eichhorn, K. J.; Voit, B.; Kremer, F. *Eur. Phys. J. E* **2005**, *17* (2), 199–202.
(18) Serghei, A.; Mikhailova, Y.; Eichhorn, K. J.; Voit, B.; Kremer, F. *J. Polym. Sci., Part B: Polym. Phys.* **2006**, *44* (20), 3006–3010.
(19) Orts, W. J.; van Zanten, J. H.; Wu, W. L.; Satija, S. K. *Phys. Rev. Lett.* **1993**, *71* (6), 867–70.
(20) Wallace, W. E.; van Zanten, J. H.; Wu, W. L. *Phys. Rev. E* **1995**, *52* (4-A), R3329–R3332.
(21) van Zanten, J. H.; Wallace, W. E.; Wu, W.-l. *Phys. Rev. E* **1996**, *53* (3), R2053–R2056.
(22) Tsui, O. K. C.; Russell, T. P.; Hawker, C. J. *Macromolecules* **2001**, *34* (16), 5535–5539.
(23) Kanaya, T.; Miyazaki, T.; Watanabe, H.; Nishida, K.; Yamana, H.; Tasaki, S.; Bucknall, D. B. *Polymer* **2003**, *44* (14), 3769–3773.
(24) DeMaggio, G. B.; Frieze, W. E.; Gidley, D. W.; Zhu, M.; Hristov, H. A.; Yee, A. F. *Phys. Rev. Lett.* **1997**, *78* (8), 1524–1528.
(25) Roth, C. B.; McNerny, K. L.; Jager, W. F.; Torkelson, J. M. *Macromolecules* **2007**, *40* (7), 2568–2574.
(26) Sills, S.; Overney Rene, M.; Chau, W.; Lee Victor, Y.; Miller Robert, D.; Frommer, J. *J. Chem. Phys.* **2004**, *120* (11), 5334–8.
(27) Forrest, J. A.; Dalnoki-Veress, K.; Stevens, J. R.; Dutcher, J. R. *Phys. Rev. Lett.* **1996**, *77* (10), 2002–2005.
(28) Forrest, J. A.; Dalnoki-Veress, K.; Dutcher, J. R. *Phys. Rev. E* **1997**, *56* (5-B), 5705–5716.
(29) Dalnoki-Veress, K.; Forrest, J. A.; Murray, C.; Gigault, C.; Dutcher, J. R. *Phys. Rev. E* **2001**, *63* (3–1), 031801/1–031801/10.
(30) Keddie, J. L.; Jones, R. A. L.; Cory, R. A. *Faraday Discuss.* **1994**, *98*, 219–30.
(31) Keddie, J. L.; Jones, R. A. L.; Cory, R. A. *Europhys. Lett.* **1994**, *27* (1), 59–64.
(32) Grohens, Y.; Brogly, M.; Labbe, C.; David, M. O.; Schultz, J. *Langmuir* **1998**, *14* (11), 2929–2932.
(33) Kawana, S.; Jones, R. A. L. *Phys. Rev. E* **2001**, *63* (2–1), 021501/1–021501/6.
(34) Pham, J. Q.; Green, P. F. *J. Chem. Phys.* **2002**, *116* (13), 5801–5806.
(35) Pham, J. Q.; Green, P. F. *Macromolecules* **2003**, *36* (5), 1665–1669.
(36) Pham, J. Q.; Mitchell, C. A.; Bahr, J. L.; Tour, J. M.; Krishanamoorti, R.; Green, P. F. *J. Polym. Sci., Part B: Polym. Phys.* **2003**, *41* (24), 3339–3345.
(37) Kim, J. H.; Jang, J.; Zin, W.-C. *Langmuir* **2001**, *17* (9), 2703–2710.
(38) Torres, J. A.; Nealey, P. F.; de Pablo, J. J. *Phys. Rev. Lett.* **2000**, *85* (15), 3221–3224.
(39) Ellison, C. J.; Torkelson, J. M. *Nat. Mater.* **2003**, *2* (10), 695–700.
(40) Long, D.; Lequeux, F. *Eur. Phys. J. E* **2001**, *4* (3), 371–387.
(41) Besancon, B. M.; Soles, C. L.; Green, P. F. *Phys. Rev. Lett.* **2006**, *97* (5), 057801/1–057801/4.
(42) Green, P. F.; Russell, T. P. *Macromolecules* **1992**, *25* (2), 783–7.
(43) Budkowski, A.; Klein, J.; Fetters, L. J. *Macromolecules* **1995**, *28* (25), 8571–8.
(44) Oslanec, R.; Brown, H. R. *Macromolecules* **2001**, *34* (26), 9074–9079.
(45) Oslanec, R.; Composto, R. J.; Vlcek, P. *Macromolecules* **2000**, *33* (6), 2200–2205.
(46) Oslanec, R.; Vlcek, P.; Hamilton, W. A.; Composto, R. J. *Phys. Rev. E* **1997**, *56* (3-A), R2383–R2386.
(47) Shull, K. R.; Kramer, E. J.; Hadziioannou, G.; Tang, W. *Macromolecules* **1990**, *23* (22), 4780–7.
(48) Shull, K. R.; Winey, K. I.; Thomas, E. L.; Kramer, E. J. *Macromolecules* **1991**, *24* (10), 2748–51.
(49) Green, P. F.; Russell, T. P. *Macromolecules* **1991**, *24* (10), 2931–5.
(50) Dai, K. H.; Kramer, E. J.; Shull, K. R. *Macromolecules* **1992**, *25* (1), 220–5.
(51) Brown, H. R. *Macromolecules* **1989**, *22* (6), 2859–60.
(52) Noolandi, J.; Hong, K. M. *Macromolecules* **1982**, *15* (2), 482–92.
(53) Leibler, L. *Macromolecules* **1982**, *15* (5), 1283–90.
(54) Leibler, L. *Physica A* **1991**, *172* (1–2), 258–68.
(55) Anastasiadis, S. H.; Gancarz, I.; Koberstein, J. T. *Macromolecules* **1989**, *22* (3), 1449–53.
(56) Birshtein, T. M.; Zhulina, E. B. *Polymer* **1989**, *30* (1), 170–7.
(57) Shusharina, N. P.; Linse, P.; Khokhlov, A. R. *Macromolecules* **2000**, *33* (10), 3892–3901.
(58) Russell, T. P.; Hjelm, R. P., Jr.; Seeger, P. A. *Macromolecules* **1990**, *23* (3), 890–3.
(59) McCoy, J. D.; Nath, S. K.; Curro, J. G.; Saunders, R. S. *J. Chem. Phys.* **1998**, *108* (7), 3023–3027.

MA071805V